PFC/JA-82-21

Bifilar Wiggler Inductance

J. Fajans

Massachusetts Institute of Technology
Cambridge, Massachusetts 02139

Bifilar Wiggler Inductance

J. Fajans

Massachusetts Institute of Technology

Cambridge. Massachusetts 02139

Abstract

Bifilar wiggler magnets are often used to produce the helical magnetic fields required for free electron laser (FEL) operation. The magnet is commonly driven by a capacitor bank. Since the wiggler field is proportional to the current in the magnet/capacitor system, it is necessary to know the inductance of the wiggler to determine the field strength. A formula for the inductance of bifilar wiggler magnets is derived and checked against ten experimental wigglers. It is found that the inductance of a typical wiggler is very low, on the order of .1 microhenries/period.

Bifilar wiggler magnets are often used to produce the helical magnetic fields required for free electron laser (FEL) operation. The magnet is commonly driven by a capacitor bank. The wiggler field is proportional to the wiggler current, and, assuming that the magnet/capacitor system is negligibly damped, the maximum wiggler current is $i_{max} = V_0/\sqrt{L/C}$. Thus the inductance of the wiggler magnet is required to predict the magnetic field stength. A sense of the inductance of a bifilar wiggler can be obtained by visualizing the wiggler as two intertwined solenoids of finite pitch and of opposite sense. Since the fields almost cancel, it is expected that the inductance of the wiggler will be quite low.

Magnetic Field

The inductance of the wiggler can be calculated from the energy identity.

$$\frac{1}{2}Li^2 = \frac{1}{2\mu_0}\int_V d^3x\,|\mathbf{B}|^2 \tag{1}$$

To solve for L, it is necessary to know $\mathbf{B}$ over all of space. A brief review of one of the methods used to calculate the magnetic field of a wiggler follows.[1] If the current in the windings of the wiggler is assumed to flow in a current sheet at radius $r = b$, then the magnetic field can be found by solving Laplace's equation for a magnetic scalar potential. Space is divided into two regions: a cylindrical region extending between the symmetry axis at $r = 0$ and the current sheet at $r = b$, and a hollow cylindrical region extending from the current sheet to infinity. Adopting the standard $\gtrless$ notation,

$$\mathbf{B} = -\nabla\Phi_{\gtrless}, \qquad \nabla^2\Phi_{\gtrless} = 0 \tag{2}$$

where $\Phi_{\gtrless}$ satisfies the normal boundary condition

$$\hat{r}\cdot\nabla(\Phi_> - \Phi_<)|_{r=b} = 0 \tag{3}$$

and the tangential boundary condition

$$-\hat{r}\times\nabla(\Phi_> - \Phi_<)|_{r=b} = \mu_0 K \tag{4}$$

where K is the current density in the current sheet.

The solution to Laplace's equation in cylindrical coordinates (r, ϕ, z) is

$$\begin{aligned}\Phi_{\gtrless} = \sum_{\nu\mu}\Big(&A^{\gtrless}_{\nu\mu}\sin\nu\phi\sin\mu z + B^{\gtrless}_{\nu\mu}\sin\nu\phi\cos\mu z \\ &+ C^{\gtrless}_{\nu\mu}\cos\nu\phi\sin\mu z + D^{\gtrless}_{\nu\mu}\cos\nu\phi\cos\mu z\Big)\mathcal{R}^{\gtrless}_{\nu}(\mu r)\end{aligned} \tag{5}$$

where

$$\mathcal{R}^{>}_{\nu}(\mu r) \equiv K_\nu(\mu r), \qquad \mathcal{R}^{<}_{\nu}(\mu r) \equiv I_\nu(\mu r) \tag{6}$$

and where I and K are modified Bessel functions.[2] Since the wiggler has right helical symmetry, it is possible to re-sum the expansion in one parameter; with θ as the new parameter, the series becomes

$$\Phi_{\gtrless} = \sum_{p=0}^{\infty}\Big(A^{\gtrless}_{p}\cos p\theta + B^{\gtrless}_{p}\sin p\theta\Big)\mathcal{R}^{\gtrless}_{p}(pk_\lambda r). \tag{7}$$

where $\theta = \phi - k_\lambda z$, $k_\lambda = 2\pi/\lambda$, and λ is the wiggler periodicity. Since current flow is odd in ϕ, it will be shown that $B^{\gtrless}_{p}$ is identically zero.

In cylindrical coordinates, the normal boundary condition (3) implies

$$0 = \sum_{p=0}^{\infty} \left(A_p^{>} K_p'(pk_\lambda r) - A_p^{<} I_p'(pk_\lambda r)\right) \cos p\theta \Big|_{r=b}, \tag{8}$$

or

$$A_p^{>} = \frac{I_p'(pk_\lambda b)}{K_p'(pk_\lambda b)} A_p^{<}. \tag{9}$$

Assuming that the current can be represented in the form

$$K = \left(\hat{\theta} + \frac{\hat{z}}{k_\lambda b}\right) \sum_{p=0}^{\infty} b_p \sin p\theta, \tag{10}$$

the tangential boundary condition (4) becomes

$$\mu_0 K = -\left(\frac{\hat{z}}{r}\frac{\partial}{\partial \phi} - \hat{\phi}\frac{\partial}{\partial z}\right)(\Phi_> - \Phi_<)\Big|_{r=b}, \tag{11}$$

or, matching the $\hat{\phi}$ terms,

$$\sum_{p=0}^{\infty} \mu_0 b_p \sin p\theta = \sum_{p=0}^{\infty} pk_\lambda \sin p\theta \left(A_p^{>} K_p(pk_\lambda r) - A_p^{<} I_p(pk_\lambda r)\right)\Big|_{r=b}. \tag{12}$$

Solving (9) and (12) for $A_p^{<}$ and using the Wronskian for modified Bessel functions yields

$$A_p^{<} = b\mu_0 K_p'(pk_\lambda b) b_p. \tag{13}$$

The standard assumption for the distribution of current in the current sheet is that the current flows in infinitesmally thin wires that can be represented by [3]

$$\tilde{K} = ik_\lambda \sum_j \left[\delta(\phi - k_\lambda z + \frac{\pi}{2} + 2\pi j) - \delta(\phi - k_\lambda z - \frac{\pi}{2} + 2\pi j)\right]. \tag{14}$$

However, this assumption leads to a logarithmic divergence in the inductance similar to the divergence of the inductance of an infinitesimally thin wire. Postulating a wire of finite thickness removes the divergence. To retain the formalism developed above, the wire will be assumed to have a thickness in the plane of the current sheet only. Experimental results presented later validate this approximation. Other authors have used different assumptions to arrive at formulas that do not correspond to the particular type of bifilar wigglar considered here.[4] Current flow is then assumed to be

$$\begin{aligned}\tilde{K} = \frac{Ik_\lambda}{\tau} \sum_j \Big\{ &\left[u(\phi - k_\lambda z + \frac{\pi}{2} + \frac{\tau}{2} + 2\pi j) - u(\phi - k_\lambda z + \frac{\pi}{2} - \frac{\tau}{2} + 2\pi j)\right] \\ &- \left[u(\phi - k_\lambda z - \frac{\pi}{2} + \frac{\tau}{2} + 2\pi j) - u(\phi - k_\lambda z - \frac{\pi}{2} - \frac{\tau}{2} + 2\pi j)\right]\Big\}\end{aligned} \tag{15}$$

where u is the unit step function and τ, the effective angular thickness in the $\hat{\phi}$ or $\hat{z}$ direction, is related to the actual wire thickness t by the formula

$$\tau = \frac{t}{b}\sqrt{1 + (k_\lambda b)^2}. \tag{16}$$

This relationship is drawn in Figure 1. Fourier transforming $\tilde{K}$ into p space yields

$$b_p = \frac{4ik_\lambda}{\pi\tau}\frac{1}{p} \sin\frac{p\pi}{2} \sin\frac{p\tau}{2}. \tag{17}$$

Substituting this result into (13) gives

$$A_p^{<} = \frac{4ik_\lambda b\mu_0}{\pi\tau}\frac{1}{p} \sin\frac{p\pi}{2} \sin\frac{p\tau}{2} K_p'(pk_\lambda b). \tag{18}$$

Inductance Calculations

Using the scalar potential derived above, it would be possible to derive the inductance from the energy identity (1) as rearranged below,

$$L = \frac{1}{i^2 \mu_0} \int_V d^3x \, |\mathbf{B}|^2 \tag{1'}$$

but this approach would involve integrals over modified Bessel functions. However, for any potential Φ satisfying Laplace's equation, Green's theorem can be written as

$$\int_V d^3x \, (\nabla \Phi)^2 = \int_S dA \, \Phi \hat{n} \cdot \nabla \Phi, \tag{19}$$

where the right hand integral is taken over the surface S surrounding the volume V. Using this identity, the inductance becomes

$$L = \frac{1}{i^2 \mu_0} \int_{S_{\substack{> \\ <}}} dA \, \Phi_{\substack{> \\ <}} \hat{n} \cdot \nabla \Phi_{\substack{> \\ <}}. \tag{20}$$

The appropriate volume for $\Phi_<$ is the infinite cylinder with radius $r = b$, while the volume for $\phi_>$ is the infinite, hollow cylinder with inner radius b and an outer radius of infinity. Since $\lim_{r \to \infty} \Phi_> \approx e^{-r}$, the surface at infinity does not contribute to the integral. Remembering that the potential is continuous across the current sheet, the inductance can be rewritten as

$$L = \frac{1}{i^2 \mu_0} \int_{r=b} dA (\Phi_< - \Phi_>) \nabla_r \Phi_<. \tag{21}$$

Using the expansions for $\Phi_<, \Phi_>$ gives

$$\begin{aligned} L = \frac{1}{i^2 \mu_0} \int_{-\lambda/2}^{\lambda/2} dz \int_{-\pi}^{\pi} r \, d\theta \sum_{p_1=1}^{\infty} \left[A_{p_1}^{<} I_{p_1}(p_1 k_\lambda r) - A_{p_1}^{>} K_{p_1}(p_1 k_\lambda r) \right] \cos p_1(\theta - k_\lambda z) \\ \times \sum_{p_2=1}^{\infty} p_2 k_\lambda A_{p_2}^{>} \cos p_2(\theta - k_\lambda z) I'_{p_2}(p_2 k_\lambda r) \Big|_{r=b}. \end{aligned} \tag{22}$$

Only the terms with $p_1 = p_2$ will survive integration, therefore

$$\begin{aligned} L = \frac{1}{i^2 \mu_0} \sum_{p=1}^{\infty} \int_{-\lambda/2}^{\lambda/2} b \, dz \int_{-\pi}^{\pi} d\theta \left[A_p^{<} I_p(p k_\lambda b) - A_p^{>} K_p(p k_\lambda b) \right] \\ \times p k_\lambda A_p^{<} I'_p(p k_\lambda b) \cos^2 p(\theta - k_\lambda z). \end{aligned} \tag{23}$$

Integrating and using the Bessel function Wronskian gives

$$L = -\frac{16 k_\lambda^2 b^2 \mu_0 \lambda}{\pi \tau^2} \sum_{p=1}^{\infty} \frac{1}{p^2} \sin^2 \frac{p\pi}{2} \sin^2 \frac{p\tau}{2} I'_p(p k_\lambda b) K'_p(p k_\lambda b). \tag{24}$$

For most wiggler magnets $k_\lambda b$ is greater than three. In this range, the approximation

$$I'_p(p k_\lambda b) K'_p(p k_\lambda b) \approx -\frac{1}{2 p k_\lambda b} \tag{25}$$

works quite well. Substituting (25) into (24) yields

$$L = \frac{16 b \mu_0}{\tau^2} \sum_{p=1}^{\infty} \frac{1}{p^3} \sin^2 \frac{p\pi}{2} \sin^2 \frac{p\tau}{2}. \tag{26}$$

A more accurate expansion for the Bessel functions* results in the following correction terms

$$L = \frac{16b\mu_0}{\tau^2}\sum_{p=1}^{\infty}\frac{1}{p^3}\sin^2\frac{p\pi}{2}\sin^2\frac{p\tau}{2}(\beta_1+\frac{\beta_2}{p^2}) \tag{27}$$

with

$$\beta_1 = 1+\frac{1}{2\alpha^2}-\frac{1}{8\alpha^4},\quad \beta_2 = \frac{1}{4\alpha^2}\left(-\frac{3}{2}+\frac{23}{4\alpha^2}\right),\quad \alpha = k_\lambda b. \tag{28}$$

As a first approximation,

$$L \approx \frac{16b\mu_0}{\tau^2}\frac{1}{2}\int_1^{\pi/\tau} dp\frac{1}{p^3}\sin^2\frac{p\tau}{2} \approx 2b\mu_0\ln\frac{\pi b}{\tau}. \tag{29}$$

The sums in (27) can be done exactly. Defining

$$S = \sum_{p=1}^{\infty}\frac{1}{p^3}\sin^2\frac{p\pi}{2}\sin^2\frac{p\tau}{2}, \tag{30}$$

trigonometric identities reduce this sum to

$$S = \frac{1}{2}\sum_{p=1}^{\infty}\frac{1}{p^3}\left(\frac{7}{8}-\cos p\tau+\frac{1}{8}\cos 2p\tau\right). \tag{31}$$

The sum $\sum_{p=1}^{\infty}1/p^3$ is defined to be the value $\varsigma(3) = 1.202$ of the Riemann Zeta Function. Defining

$$S = \sum_{p=1}^{\infty}\frac{1}{p^3}\cos\gamma p, \tag{32}$$

and taking two derivatives with respect to γ gives

$$S'' = -\sum_{p=1}^{\infty}\frac{1}{p}\cos\gamma p. \tag{33}$$

This sum is tabulated:[6]

$$S'' = \frac{1}{2}\ln\left(4\sin^2\frac{\gamma}{2}\right) \approx \ln\gamma-\frac{\gamma^2}{24} \tag{34}$$

since γ is small. Integrating twice gives

$$S = \varsigma(3)+\gamma^2\left(\frac{\ln\gamma}{2}-\frac{3}{4}-\frac{\gamma^2}{288}\right). \tag{35}$$

Substituting (35) into (31) yields

$$S = \frac{\tau^2}{8}\left(\ln\frac{1}{\tau}+\frac{3}{2}+\ln 2-\frac{\tau^2}{72}\right). \tag{36}$$

The sum appropriate for β_2 can similarly be shown to be

$$S_2 = \sum_{p=1}^{\infty}\frac{1}{p^5}\sin^2\frac{p\pi}{2}\sin^2\frac{p\tau}{2} \approx \frac{1}{8}\varsigma(3)\tau^2. \tag{37}$$

Therefore the inductance of a wiggler magnet in units of henries/wiggler period and where all length dimentions are given in meters is

$$L = 2b\mu_0\left\{\beta_1\left(\ln\frac{1}{\tau}+\frac{3}{2}+\ln 2-\frac{\tau^2}{72}\right)+\beta_2\varsigma(3)\right\}. \tag{38}$$

*The large z expansion is: $I_p'(z)K_p'(z) \approx -\frac{1}{2z}\left(1+\frac{1}{2}\frac{\mu-3}{(2z)^2}-\frac{1}{8}\frac{(\mu-1)(\mu-45)}{(2z)^4}+\cdots\right)$ where $\mu = 4p^2$. [5]

where $\varsigma(3) = 1.202$ and

$$\beta_1 = 1 + \frac{1}{2\alpha^2} - \frac{1}{8\alpha^4}, \quad \beta_2 = \frac{1}{4\alpha^2}\left(-\frac{3}{2} + \frac{23}{4\alpha^2}\right), \quad \alpha = k_\lambda b, \tag{28}$$

$$\tau = \frac{t}{b}\sqrt{1 + (k_\lambda b)^2}. \tag{16}$$

In most cases an adequate approximation is obtained by setting $\beta_1 = 1$, $\beta_2 = 0, \tau = tk_\lambda$ and ignoring the τ^2 term.

Experimental Results

The inductance of ten wigglers was found experimentally and compared to the theoretically predicted inductance. The inductance was measured by determining the voltage drop across the wiggler when the wiggler was driven by a sinusoidal current of known magnitude and frequency. Because the inductance of a typical wiggler is very low, it was necesary to use frequencies in the megahertz range. Each wiggler was measured at at least four frequencies, and the average value was used. Because of the effects of internal resistance and non-negligible capacitance, the experimental error was about fifteen percent. In practice, the wigglers would be run at frequencies around one kilohertz where skin effects would probably cause systematic differences between the measured, high frequency inductance and the practical inductance. The radius b of the windings, the period λ, and the thickness of the wires was measured and used to calculate the predicted inductance.

The table below lists the wiggler parameters and their experimental and calculated inductances. The last two wigglers used cylindrical wires. The other wigglers had wires of rectangular cross section, and the widest dimension was used as the wire thickness. Two of the wigglers (II,X) were very short and consequently show small, but not negligible, deviations due to end effects. Figure 2 is a scatter plot of the parameters, while Figure 3 plots the experimental inductances against the calculated inductances. Figure 4 is a contour plot of the theoretical inductance against the radius of the windings and the period for a fixed wire thickness.

Inductance Tests						
Wiggler Type	b cm	λ cm	t cm	Periods	L_{exp} microhenries/period	L_{calc} microhenries/period
I	3.35	2.25	.250	20	.213	.215
II	3.35	2.25	.250	4	.270	.215
III	3.35	.800	.250	20	.143	.123
IV	3.35	1.50	.250	20	.174	.180
V	2.13	1.51	.178	35	.163	.130
VI	2.13	1.23	.178	35	.145	.122
VII	2.13	.643	.178	35	.107	.086
VIII	1.87	5.05	.178	9.5	.182	.184
IX	1.10	.854	.203	61	.033	.048
X	2.06	3.17	.318	8.25	.095	.139

Acknowledgements

This work was supported in part by the National Science Foundation and in part by the Hertz Foundation.

References

[1] Paul Diament, "Electron Orbits and Stability," *Physical Review A.* 23, (1981), 2539-2541.

[2] J. D. Jackson, *Classical Electrodynamics*, Wiley, New York, (1975), 107-8.

[3] Diament, 2540.

[4] Chester Snow, *Formulas for Computing Capacitance and Inductance*, National Bureau of Standards Circular 544, Washington, (1954).

[5] *Handbook of Mathematical Functions*, Abramowitz & Stegun, eds. National Bureau of Standards, Washington, (1972), 378.

[6] Gradshteyn & Ryzhik, *Table of Integrals, Series, and Products*, Academic Press, New York, (1980), 38.

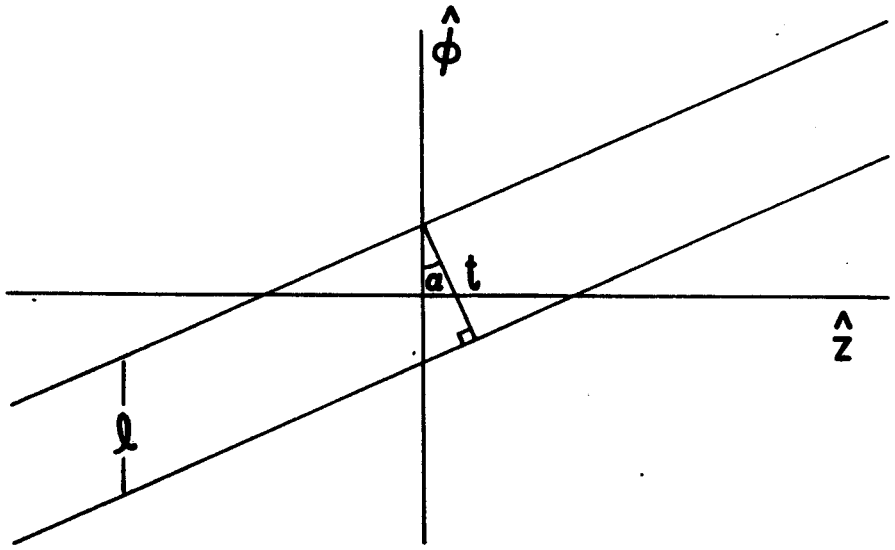

Figure 1. Relationship between τ and t. Here $\tau = l/b = t/b\cos\alpha$, $\tan\alpha = k_\lambda b$, and b is the winding radius.

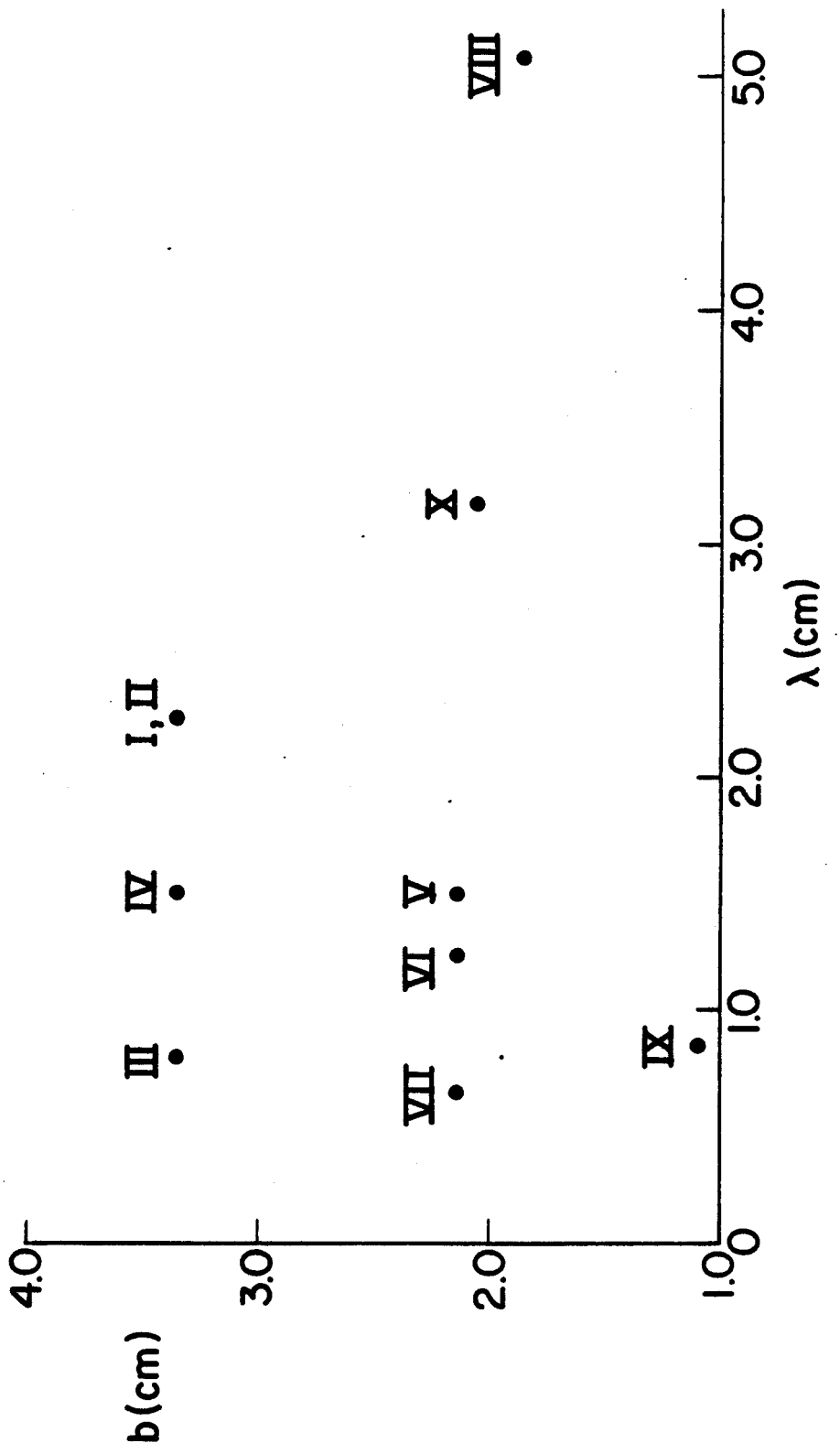

Figure 2. Scatter plot showing the dimensional parameters of the experimental wigglers.

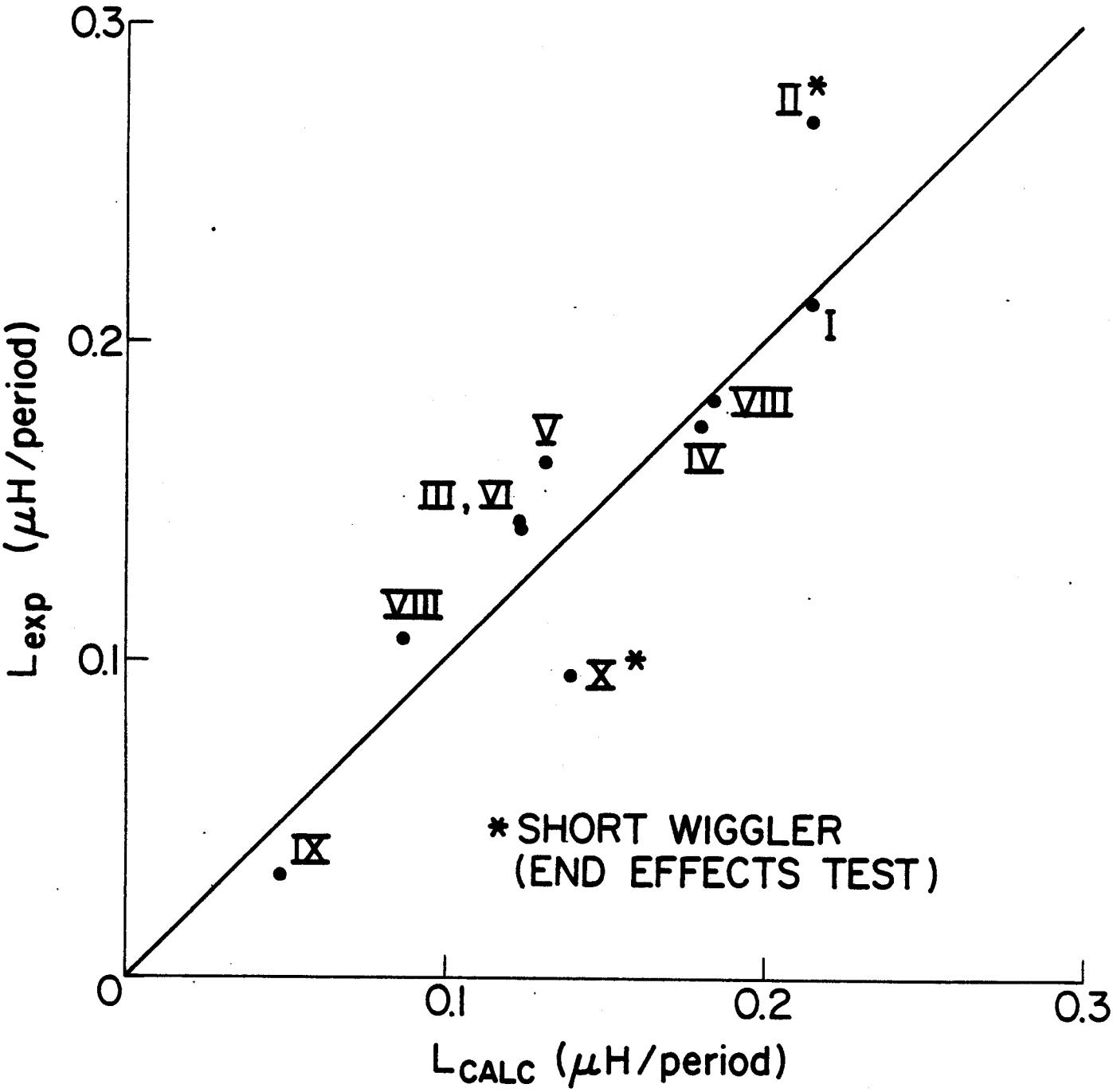

Figure 3. Calculated vs. Experimental inductance for the experimental wigglers.

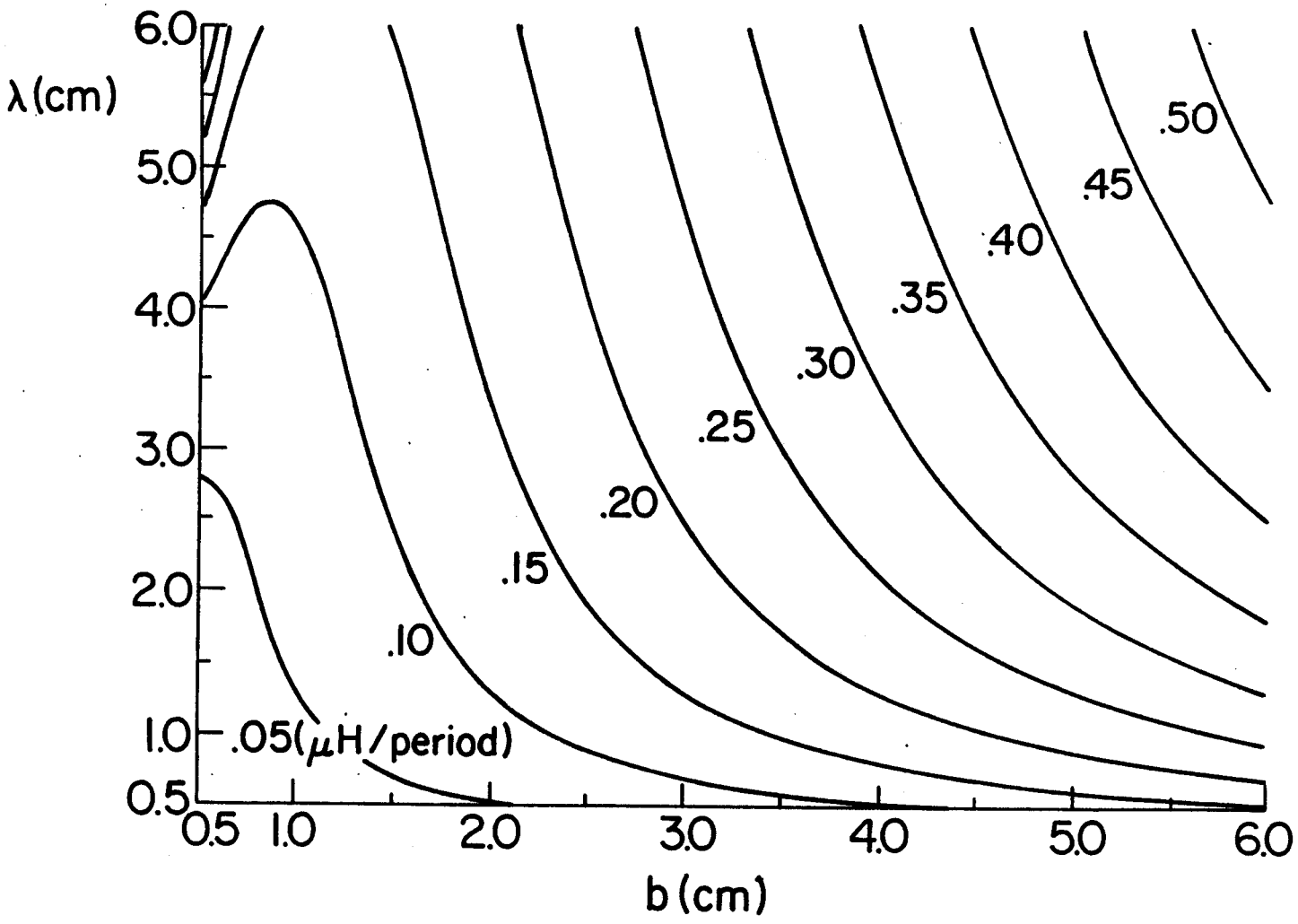

Figure 4. Contour plot of b and λ vs. wiggler inductance.